Flow cytometry allows rapid detection of protein aggregates in cellular and zebrafish models of spinocerebellar ataxia 3

Katherine J Robinson[1], Madelaine C. Tym[1], Alison Hogan[1], Maxinne Watchon[1], Kristy C Yuan[1], Stuart K Plenderleith[1], Emily K Don[1] and Angela S Laird[1,*]

[1]Centre for Motor Neuron Disease Research, Department of Biomedical Sciences, Faculty of Medicine, Health and Human Sciences, Macquarie University, Sydney Australia

* Correspondence: angela.laird@mq.edu.au

Abstract: Spinocerebellar ataxia-3 (SCA3, also Machado Joseph disease), is a neurodegenerative disease caused by inheritance of a CAG repeat expansion within the *ATXN3* gene, resulting in polyglutamine (polyQ) repeat expansion within the ataxin-3 protein. In this study we have identified protein aggregates in both neuronal-like (SHSY5Y) cells and transgenic zebrafish expressing human ataxin-3 with expanded polyQ. We have adapted a previously reported flow cytometry methodology named flow cytometric analysis of inclusions and trafficking (FloIT), allowing rapid quantification of detergent insoluble forms of ataxin-3 fused to a green fluorescent protein in the SHSY5Y cells and cells dissociated from the zebrafish larvae. Flow cytometric analysis revealed an increased number of detergent-insoluble ataxin-3 particles per nuclei in the cells and zebrafish expressing polyQ expanded ataxin-3 compared to those expressing wildtype human ataxin-3. Treatment with compounds known to modulate autophagy activity was found to alter the number of detergent-insoluble ataxin-3 particles in cells and zebrafish. We conclude that flow cytometry can be harnessed to rapidly count ataxin-3 aggregates, both *in vitro* and *in vivo*, and can be utilised to compare potential therapies targeting protein aggregates.

Keywords: Spinocerebellar ataxia-3; Machado Joseph disease; hereditary spinocerebellar ataxias; neurodegenerative disease; flow cytometry; proteinopathy; insoluble protein species; protein aggregates

Abbreviations: SCA3, spinocerebellar ataxia-3; MJD, Machado Joseph Disease; polyQ, polyglutamine, EGFP, enhanced green fluorescent protein; dpf, days post-fertilisation; FloIT, flow cytometric analysis of inclusions and trafficking; DAPI, 4',6-diamidino-2-phenylindole; 3MA, 3-methyladenine; ANOVA, analysis of variance.

Introduction

Spinocerebellar ataxia-3 (SCA3, also known as Machado Joseph Disease or MJD) is a devastating neurodegenerative disease that causes progressive ataxia (loss of balance and co-ordination) and paralysis, as well as impaired speech, swallowing and vision due to the progressive death of neurons in the central nervous system [1]. SCA3 is the most common form of hereditary ataxia found throughout the world (21-28% of autosomal-dominant ataxia) [2-4], affecting approximately 1-5 per 100 000 people worldwide.

SCA3 is caused by inheritance of an abnormal form of a gene called *ATXN3* [5, 6]. The *ATXN3* gene normally contains a repetitious sequence of genetic code (CAG repeat region), which in turn encodes a long string of glutamine (Q) residues (known as a polyQ region) within the ataxin-3 protein. Whilst the normal (wild-type) ataxin-3 protein contains 12-44 glutamine residues within the polyQ region, expression of ataxin-3 with more than 44 glutamine residues produces SCA3 disease in patients [1, 7]. A direct relationship exists between the length of this polyQ region and the severity of SCA3, with patients carrying longer repeat lengths suffering earlier disease onset, more severe disease and earlier death [7-10].

Neuropathological staining of SCA3 patient brain samples often reveals the presence of ataxin-3-positive neuronal intranuclear inclusions [11]. Formation of these ataxin-3 protein aggregates and inclusions is hypothesized to play a role in the neuronal dysfunction and degeneration that occurs in SCA3 [11-13]. Whilst the ataxin-3 protein has been found to function as a de-ubiquinating enzyme [14], ataxin-3 has also been found to sequester other essential proteins into protein aggregates, altering the essential functions of sequestered proteins [15, 16]. Similarly, other proteins containing polyglutamine tracts, such as huntingtin and the androgen receptor, have also been found to aggregate when the polyglutamine tract is expanded, resulting in neurodegenerative diseases such as Huntington's disease and Kennedy's disease, respectively [17, 18]. For these reasons, approaches to identify therapeutics that can prevent, or reverse, protein aggregation processes are currently an area of thorough investigation within the field [19].

Whiten et al [20] previously established a flow cytometric approach enabling rapid enumeration of insoluble protein inclusions per nuclei present in cell culture models, coined flow cytometric analysis of inclusions and trafficking (FloIT). This approach has since been used to rapidly quantify the number of detergent insoluble inclusions across many *in vitro* models expressing aggregation-prone proteins, including mutant huntingtin (linked with Huntington's disease) [20] and motor neuron disease-linked proteins mutant SOD1 [20, 21] and TDP-43 [22, 23]. The application of FloIT has also been expanded to investigate other cellular processes associated with protein aggregation, including induction of a heat shock response [24], the role of molecular chaperones in suppressing protein aggregation [25] and chaperone-assisted selective autophagy [26]. Considering that formation of detergent-insoluble protein aggregates is a disease mechanism common to a wide variety of diseases, including Alzheimer's disease, Parkinson's disease, polyglutamine diseases such as Huntington's disease and spinocerebellar ataxias, and even type 2 diabetes and dilated cardiomyopathy [26-31], it is important to determine whether FloIT can be widely adopted to study other proteinopathy disease models. This is especially important to determine when considering proteinopathies within differing cellular compartments. For example, protein aggregates found in models of motor neuron disease and Huntington's disease are more commonly present within the cell cytoplasm, whilst in other diseases, like forms of spinocerebellar ataxia, protein aggregates can also be detected within the cell nucleus.

In the present study, we demonstrate that FloIT can be adapted to quantify the number and size of detergent-insoluble EGFP-fused ataxin-3 particles in neuronal-like (SHSY5Y) cells transiently expressing ataxin-3 containing a short polyQ region length (28 glutamine residues) or long polyQ region length (84 glutamine residues). We also report adaption of this methodology for use with our previously reported transgenic zebrafish model of SCA3 [32]. This adaption is important because zebrafish are an excellent model for moderate to high throughput assessment of drug efficacy, as overexpression of human genes can produce disease phenotypes akin to human disease phenotypes, including impaired movement, within days. Further, potential therapeutic compounds can be diluted into the water the fish live in and easily absorbed [33]. This is the first report of use of such an approach with an *in vivo* model and provides a novel tool to assess efficacy in drug testing studies investigating treatments for proteinopathy diseases.

Materials and Methods

SCA3 Cell Culture Models

Human neuroblastoma (neuronal-like) SHSY5Y cells were grown under sterile conditions and maintained at 37°C in a sterile incubator. Cells were grown in DMEM/Nutrient Mixture F12 Ham and supplemented with 10% fetal bovine serum and 5% CO_2. Cells were seeded into 6-well plates and allowed to grow for 1-3 days until 80-90% confluent. Once confluent, cells were transiently transfected with vectors to drive expression of EGFP fused to human ataxin-3 with a short polyQ repeat length (28Q) or human ataxin-3 with an expanded polyQ repeat length (84Q) or an EGFP only vector control. Cells were transfected with 1 µg of DNA and 1 µL of Lipofectamine 2000 (Thermo Fisher) per well and incubated for 24 hours.

Confocal microscopy of aggregates in a SHSY5Y cell model of SCA3

For confocal imaging experiments, SHSY5Y cells were seeded into a 24 well-plate and grown on coverslips until reaching 60-70% confluency. Cells were then transfected with 1 µL of Lipofectamine 2000 and 1 µg of DNA per well. At 24 hours post-transfection, culture media was aspirated, and cells were fixed with 4% paraformaldehyde and stained with 4',6-diamidino-2-phenylindole (DAPI, final concentration 14 µM) to enable identification of nuclei, then mounted using fluorescent mounting media (Dako Omnis, Aglient catalogue # GM304). Confocal images were obtained using a Zeiss LSM-880 confocal microscope (Plan-Apochromat 40x/1.5 oil DIC M27 objective) running Zen Black software (Zeiss, Gottingen, Germany). In order to visualise EGFP expression, an argon laser was used. To visualise DAPI-stained nuclei, a 405 nm laser was used. A total of six z-stack images (13 slices spanning 6 µm) of different fields of view were acquired per coverslip and final images were obtained as maximum intensity projections using Fiji software software [34]. EGFP-positive aggregates were manually counted by a researcher blind to experimental group. The number of aggregates per transfected cell was then calculated by averaging the results from six fields of view per coverslip.

Preparation of SCA3 cell cultures for FloIT

For flow cytometry experiments, SHSY5Y cells were seeded into 6-well plates and prepared for flow cytometry 24-hours post-transfection. Cultured SHSY5Y cells were imaged with 20x objective using an EVOS microscope (Invitrogen, catalogue number AMF4300) under brightfield and GFP LED light cube to determine transfection efficiency prior to harvesting. The total number of cells and total number of GFP-expressing cells were counted using automated cell counting functions within Fiji, allowing calculation of transfection efficiency. Cells were briefly washed in PBS and harvested using 0.5% trypsin-EDTA and pelleted. Pelleted cells were re-suspended in lysis buffer (phosphate buffered saline containing 0.5% Triton-X 100 and complete protease inhibitors [Roche]) and DAPI was added (final concentration 5 μM) to allow enumeration of the number of nuclei. The use of DAPI to quantify nuclei aligns with experiments from Adriaenssens, Tedesco [26] but contrasts with many previous reports of FloIT [20-22]. Samples were incubated on ice and protected from light until analysis. All samples underwent flow cytometric analysis within 30 minutes of lysis with Triton-X 100.

Transgenic SCA3 Zebrafish

The present study utilised a previously described zebrafish model of SCA3 [32]. Within these studies we used embryos resulting from crossing zebrafish driver line mq15: Tg(elavl3:Gal4-VP16; mCherry) with either line mq16: Tg(UAS:Hsa.ATXN3_23xCAG-EGFP,DsRed) or mq17: Tg(UAS:Hsa.ATXN3_84xCAG-EGFP,DsRed), resulting in transgenic zebrafish neuronally expressing both dsRED and EGFP-fused ATXN3 with either short (23Q) or long (84Q) polyQ lengths, respectively. In the present study, all breeding was performed by in-crossing F1 transgenic males with F1 transgenic females expressing both driver and reporter lines with no out-crossing to wildtype zebrafish. All animal experiments were performed in accordance with the Code and approved by the Animal Ethics Committee of Macquarie University (2016/004) and the Biosafety Committee of Macquarie University (Notifiable Low Risk Dealing: 5974). Zebrafish were housed in a standard recirculating aquarium system maintained at 28.5^{o}C. Zebrafish embryos were screened for fluorescence (EGFP and

dsRED) at 1-day post-fertilisation (1 dpf) indicating expression of transgenic lines. Embryos were dechorionated and housed in 6-well plates (15-25 larvae per well, housed at equal densities per group).

Imaging of aggregates in a transgenic zebrafish model of SCA3

At 6 days post-fertilisation (6 dpf), transgenic zebrafish were anaesthetised with 0.01% Tricaine (Sigma, catalogue number E10521) and embedded in 1% low-melting agarose (Sigma, catalogue number A4018). Confocal imaging was performed using an upright Leica SP5 confocal microscope (40x water submersible objective). An argon laser (39% laser power) was used to excite EGFP. Z-stacks spanning the depth of the spinal cord (~10 µm) were acquired and final images were obtained as maximum intensity projections using or Fiji software [34]. EGFP positive aggregates were manually counted and the aggregate size measured by a researcher blind to experimental group.

Western Blotting

SHSY5Y cells transiently expressing EGFP, EGFP-fused human ataxin-3 with 28 glutamines or EGFP-fused human ataxin-3 with 84 glutamines were harvested for protein extraction and lysed using ice-cold RIPA solution containing protease inhibitors (Complete ULTRA tablets, Roche) and phosphatase inhibitors (PHOSstop tablets, Roche). Cells were incubated in RIPA for 20 minutes (gently shaking) before manual scraping was used to harvest cells. To extract protein from 2 dpf zebrafish larvae, zebrafish larvae were euthanised and homogenised in RIPA solution (0.5 µL per larvae) containing protease inhibitors (Complete ULTRA Tablets, Roche), using a manual dounce.

Cellular debris was removed from protein homogenates via centrifugation (20 minutes at 13200 RPM, 4^{o}C). Protein concentration of the cleared supernatant was determined using Pierce™ BCA Protein Assay Kit (Thermo Fisher Scientific). Proteins were denatured by boiling at 95°C for 5 minutes in 1x Laemelli's buffer (Biorad) with 1x NuPAGE Reducing Agent (Life Technologies). Equal amounts of denatured proteins (20 µg) were loaded and separated by gel electrophoresis using 4-15% Tris-glycine gels (Biorad). Separated proteins

were then transferred to a PVDF membrane (0.45 µm pore size) for immunoblotting. Immunoblots were probed with primary antibodies against human ataxin-3 (produced in rabbit, gift from H. Paulson) and GAPDH (produced in mouse, Proteintech). Immunoblots were probed with appropriate horseradish peroxidase secondary antibodies (Promega) and visualised by chemiluminescence (Supersignal detection kit, Pierce) using an ImageQuant LAS4000 imaging system.

Preparation of Dissociated of Zebrafish Larvae for Flow Cytometry

Dissociation of whole zebrafish was adapted from methods previously described by Acosta, Watchon [35]. In brief, whole zebrafish larvae (2 or 6 dpf) were euthanised and larvae bodies were manually transferred to a petri dish in a droplet of E3 media and manually dissected into pieces (<1 mm) using a scalpel blade. Larvae pieces were then transferred to an Eppendorf tube and centrifuged. The supernatant was removed and the pellet was enzymatically digested using 0.5% Trypsin-EDTA (500 µL for 2dpf larvae, 1000 µL for 6dpf larvae) for 30 minutes at 37^{o}C. Samples were vortexed frequently to aid digestion. Trypsinisation was stopped by the addition of 1 mL of DMEM cell culture media containing 10% fetal bovine serum. Samples were pelleted and the DMEM/trypsin solution was removed. Samples were resuspended in 200 – 500 µL of PBS containing 0.5% Triton-X and 1 x RedDot^{TM} far red solution (Gene Target Solutions, catalogue number 40060) to identify nuclei.

In order to confirm that cells could survive the dissociation process, a subset of experiments were performed whereby dissociated cells were not used for flow cytometry and instead were stained with Hoechst 33342 live cell stain (Thermo Fisher, final concentration 400 µM) and imaged using an EVOS microscope (20x objective). The total number of cells and total number of Hoechst -positive cells were counted using Fiji automated cell counting functions, allowing calculation of cell survival post-dissociation (Supplementary Figure 1A).

Drug treatments in SCA3 cell cultures and transgenic SCA3 zebrafish

As a proof of principle, we examined the effect of prior treatment with compounds known to alter activity of the autophagy protein quality control pathway on the number of detergent-insoluble ataxin-3 particles detected using flow cytometry, in SCA3 cell cultures

and transgenic zebrafish. For autophagy inhibition experiments, cultured cells were treated with 3-methyladenine (3MA, 5 mM, Cayman Chemicals [catalogue number 13121]) and zebrafish larvae were treated with chloroquine diphosphate (3 mM, Sigma-Aldrich [catalogue number C6628]), two commonly utilised inhibitors of autophagy [36]. To examine the effect of autophagy induction on detergent-insoluble ataxin-3, calpeptin (Caymen Chemicals [catalogue number 14593]), a compound known to induce autophagy in SCA3 zebrafish [32] and suppress protein aggregation in cell culture [37, 38], was administered at doses ranging from 1 - 5 μM in cell culture and 25 μM – 100 μM for zebrafish. For drug treatments of SHSY5Y cells transiently expressing human ataxin-3, 3MA or calpeptin treatments were dissolved in culture media (DMEM/Nutrient Mixture F12 Ham and supplemented with 10% fetal bovine serum) and applied immediately prior to the addition of transfection reagents. For drug treatments of transgenic zebrafish, chloroquine diphosphate or calpeptin were diluted in E3 raising media and larvae were placed in drug treatments for a minimum of 24 hours. All drug treatments were dissolved in dimethyl sulfoxide (DMSO) to create stock solutions. The final maximum percentage of DMSO for cell culture drug treatments reached 0.003%, whilst zebrafish experiments did not exceed a final maximum percentage of 0.01%. Stock solutions were aliquoted and stored at -20^{o}C. Treatment with DMSO alone acted as the vehicle control and the effect of all examined drug treatments were directly compared to vehicle treated controls.

Flow Cytometry Analysis Approach

Flow cytometry was performed using a Becton Dickson Biosciences LSR Fortessa analytical flow cytometer running FACS DIVA software and maintained according to manufacturer's instructions (Becton Dickson). Excitation wavelengths and emission collection windows were set as follows: DAPI (355nm, 525/50nm), EGFP (488nm, 530/30nm) and RedDot^{TM} (640nM, 670/30nm). A minimum of 20,000 events were captured for experiments involving culture cells and 50,000 events were captured for experiments involving dissociated cells from whole zebrafish larvae. The fluorescence of EGFP-expressing cells was compared to an un-transfected or non-transgenic control sample. Nuclei were identified and quantified based on intensity of UV/infrared fluorescence and particle size (forward scatter). The number of detergent-insoluble EGFP particles, indicating insoluble EGFP-fused ataxin-3 particles, were analysed based on GFP fluorescent intensity and forward scatter [20]. For genotype comparisons, the number of detergent-insoluble EGFP-positive particles was determined

using the FloIT equation published by Whiten and colleagues [20]: 100 x (# of Insoluble GFP Particles/ # nuclei x transfection efficiency). This analysis approach allows for comparison of detergent-insoluble particles across different transgenic expression models. For comparison of treatment effects on the same transgenic model, the number of detergent-insoluble EGFP-positive particles per number of nuclei present was calculated and presented as a fold-change relative to the vehicle treated control group. The FSC threshold was set to 200 AU (AU, arbitrary units) to ensure small insoluble particles were included in the analysis. Axes were set to $\log^{10}$ for all experiments. Non-fluorescent microspheres (Thermo Fisher, catalogue number F13838) of a known diameter (1 – 15 µm) were used to equate forward scatter measurements (AU) to a precise micron diameter (Supplementary Material Figure 1B).

Data analysis

Data analysis was performed using GraphPad Prism (Version 8) software. Group comparisons were made using one-way ANOVA tests, followed by a Tukey post-hoc to identify differences. In cases where only two groups were compared, comparisons were made using a student t-test. All graphs display group mean data ± standard error mean.

Results

Expression of human ataxin-3 with an expanded polyglutamine region in neuronal-like SHSY5Y cells results in the formation of EGFP-positive aggregates

Microscopic analysis of SHSY5Y cells expressing EGFP fused-human ataxin-3 containing 28Q (EGFP-ataxin-3 28Q), EGFP-ataxin-3 84Q or EGFP alone, revealed the presence of more frequent EGFP-positive aggregates within the cells expressing human ataxin-3 containing 84Q than 28Q or EGFP-only vector control (Figure 1A). Manual counting of the number of EGFP-positive protein aggregates and one-way analysis of variance revealed a significant difference in the number of EGFP-positive aggregates across genotypes ($p < 0.0001$). Post-hoc comparisons revealed that more aggregates were present in the SHSY5Y cells expressing EGFP-ataxin-3 84Q when compared to cells expressing EGFP alone ($p < 0.0001$) or EGFP-ataxin-3 28Q ($p = 0.0002$; Figure 1B). Further, analysis of manual counts revealed a difference in the number of cells affected with protein aggregates across

genotypes ($p < 0.0001$, Figure 1C). Multiple comparisons revealed that cells transiently expressing EGFP-fused ataxin-3 84Q displayed a significantly higher percentage of cells harbouring EGFP-positive aggregates than cells expressing EGFP only ($p < 0.0001$) and cells expressing EGFP-fused ataxin-3 with 28Q ($p = 0.0033$).

Next, we used western blotting to examine the relative expression of ataxin-3 across our three cell culture expression models, as the relative amount of protein expressed could influence ataxin-3 aggregation. Immunoblot analysis of SHSY5Y cells transiently expressing EGFP-fused human ataxin-3 or an EGFP only control revealed expression of endogenous ataxin-3 and overexpression of EGFP-fused human ataxin-3 (Figure 1D, see Supplementary Figure 2A for full immunoblot). The expression of EGFP-fused human ataxin-3 was found to differ across examined genotypes ($p < 0.0001$, Figure 1E), with expression human ataxin-3 found to be higher in cells expressing EGFP-fused ataxin-3 28Q and ataxin-3 84Q when compared to cells expressing EGFP only ($p < 0.0001$ and $p = 0.0001$, respectively). Interestingly, the expression of EGFP-fused ataxin-3 28Q was found to be significantly increased when compared to the expression found in ataxin-3 84Q expressing cells ($p < 0.0001$), suggesting the increased presence of ataxin-3 aggregates in our MJD cells is not due to underlying differences in protein expression.

We next validated the rapid quantification of the number Triton-X 100 insoluble aggregates using the previously reported FloIT methodolgy [20]. Transfected cells underwent flow cytometric analysis to quantify the number and size of Triton-X insoluble particles (Figure 2A). Firstly, fluorescent microscopy was used to confirm the number of transfected cells per sample (prior to harvesting). The calculated transfection efficiency of each sample was utilised to calculate the total number of detergent-insoluble particles per sample. Next, the total number of nuclei present within the lysed sample was determined by a DAPI stain for nuclei. The number of DAPI-positive particles was quantified using population gating based on intensity of UV fluorescence and relative size (forward scatter). No statistically significant differences in the number of DAPI-positive nuclei were detected across examined groups ($p = 0.996$, Figure 2B). The number of Triton-X 100 insoluble EGFP-positive particles was then identified via gating of particle populations present within cells expressing EGFP constructs but absent in the untransfected control sample [20]. The number of Triton-X insoluble EGFP-positive particles was calculated using the FloIT equation: 100 x (# of Insoluble GFP Particles/ # DAPI nuclei x transfection efficiency) as previously reported by Whiten, San Gil [20]. This equation revealed a statistically significant

difference across the analysed genotypes (one-way ANOVA: $p = 0.0013$, n = 4-9 experimental replicates per group), with a greater number of detergent-insoluble particles per 100 cells found in EGFP-ataxin-3 84Q-expressing SH-SY5Y cells when compared to cells expressing EGFP alone ($p = 0.0022$) and EGFP-ataxin-3-28Q ($p = 0.0118$) (Figure 2C). No significant differences were found between the number of detergent-insoluble particles expressed in EGFP alone or EGFP-ataxin-3-28Q ($p = 0.4328$). Additionally, use of non-fluorescent microspheres of known size allowed us to identify that EGFP-ataxin-3-84Q cells harbored detergent-insoluble particles that were similar in size to cells expressing EGFP-ataxin-3-28Q and EGFP alone (Figure 2D).

Treatment of SCA3 cell cultures with compounds known to modulate autophagic activity altered the number of EGFP-fused ataxin-3 particles detected by FloIT

In order to validate the use of FloIT as a tool to screen the effect of compounds on detergent-insoluble protein species proteinopathy, we treated cells transiently transfected with EGFP-ataxin-3 84Q for 24 hours with 3MA, a known inhibitor of autophagy [36, 39], and calpeptin, a compound known to induce autophagy and reduce proteinopathy in polyQ disease models [32, 38, 40]. Indeed, we found that 24-hour treatment with modulators of the autophagy protein quality control pathway altered the number of EGFP particles detected by flow cytometry (Figure 3A). We found that treatment with 3MA did not alter the number of DAPI-positive nuclei detected within each sample ($p = 0.838$, Figure 3B). In contrast, treatment with 3MA produced a 1.3-fold increase in the number detergent-insoluble EGFP particles present within cells expressing EGFP-ataxin-3 84Q when compared to vehicle treatment ($p = 0.002$, Figure 3C). Next, we examined the effect of increasing doses of calpeptin, a known autophagy inducer, on the number of Triton-X insoluble particles detected in cell culture samples transfected with EGFP ataxin-3 84Q (Figure 3D). Calpeptin treatment did not alter the number of nuclei detected within each sample ($p = 0.438$, Figure 3E), however calpeptin was found to alter the number of detergent-insoluble EGFP particles detected ($p = 0.028$, Figure 3F). Post-hoc comparisons revealed that treatment with 1 µM calpeptin did not significantly alter the number of insoluble particles detected when compared to vehicle treatment ($p = 0.331$). In contrast, treatment with 2.5 µM or 5 µM calpeptin produced a statistically significant decrease in the number of detergent-insoluble particles, compared to vehicle treatment ($p = 0.021$ and $p = 0.031$, respectively.

Expression of expanded human ATXN3 in transgenic zebrafish results in the formation of ataxin-3-positive aggregates

We have previously described a transgenic zebrafish model of SCA3 that overexpresses EGFP-fused human ataxin-3 with expanded polyQ (84Q) tract, that develops impaired swimming behaviour and shortened lifespan [32]. Furthermore, histological analysis of the medulla from adult zebrafish (12 months of age) expressing human mutant ataxin-3 (84Q) evidenced a neuritic beading pattern, that is the presence of ataxin-3 protein aggregates in neuronal neurites, which was positive for both ataxin-3 and ubiquitin [32]. In this current study we performed confocal microscopy on transgenic zebrafish larvae expressing human ataxin-3 at 6 dpf to examine the rostral spinal cord (Figure 4A). We observed similar levels of overall human ataxin-3 expression in zebrafish expressing ataxin-3 with 23 glutamine residues and ataxin-3 with 84 glutamine residues and observed EGFP-positive protein aggregates in neurons in both transgenic models. Manual counting of the EGFP-positive protein aggregates identified a statistically signficntly higher number of aggregates in larvae expressing EGFP-ataxin-3-84Q than in EGFP-ataxin-3-23Q ($p = 0.0007$; n = 5 zebrafish larvae imaged per ataxin-3 construct, Figure 4B). In addition to quantifying the number of aggregates present per zebrafish, we also quantified the percentage of neurons that harboured EGFP-positive protein aggregates. Transgenic MJD zebrafish were found to possess a significantly higher percentage of cells harbouring ataxin-3 aggregates when compared to zebrafish expressing EGFP ataxin-3 23Q ($p = 0.0004$, Figure 4C). Measurement of the size of observed protein aggregates within our maximum intensity microscopy images revealed that transgenic zebrafish expressing EGFP ataxin-3 23Q had significantly smaller aggregates (approximately 1 μm) compared to zebrafish expressing EGFP ataxin-3 84Q (containing aggregates greater than 2 μm in diameter) (Figure 4D).

In order to confirm that the increase presence of ataxin-3 aggregates in transgenic MJD zebrafish was not due to underlying differences in protein expression, protein lysates from 2 dpf zebrafish were obtained and immunoblotted to examine ataxin-3 expression. Immunoblotting revealed the presence of endogenous zebrafish ataxin-3, full length EGFP-fused human ataxin-3 and the presence of cleaved human ataxin-3 species (Figure 4E, see Supplementary Figure 2B for full immunoblot). Densiometric analysis revealed a statistically significant difference in the expression of human ataxin-3 across examined genotypes ($p = 0.0043$, Figure 4F). Post-hoc comparisons revealed significantly higher expression of human ataxin-3 in transgenic zebrafish expressing EGFP ataxin-3 23Q or

EGFP ataxin-3 84Q when compared to non-transgenic siblings ($p = 0.0037$ and $p = 0.0428$, respectively). No statistically significant differences were detected in the expression of human ataxin-3 between EGFP ataxin-3 23Q and EGFP ataxin-3 84Q expressing larvae ($p = 0.381$). These findings align with our previous reports of similar levels of ataxin-3 in this same transgenic zebrafish line at 3 dpf and 6 dpf [32].

Flow cytometry can be utilised to quantify number of ataxin-3 protein aggregates in transgenic zebrafish

We then modified the FloIT approach to allow quantification of the number of detergent-insoluble EGFP-positive protein aggregates within cells dissociated from whole zebrafish larvae (2 or 6 dpf) expressing human EGFP-fused ataxin-3. Following euthanasia, manual dissection and trypsinisation of whole zebrafish larvae bodies resulted in a suspension of dissociated cells that could then be lysed with 0.5% Triton-X and detergent-insoluble populations were examined using FloIT (Figure 5A). Visualisation of lysed particles using an infrared laser (excitation 640 nm, emission 670 nm) revealed similar numbers of RedDot™ labelled nuclei present within 2 dpf samples ($p = 0.905$, Figure 5B) confirming equal number of cells per sample. In contrast, visualisation of particles using blue-green laser (excitation 488 nm, emission 525 nm) revealed the presence of detergent-insoluble EGFP-positive populations in the cells dissociated from the zebrafish larvae. These EGFP-positive aggregates were detectable as early as two days post-fertilisation, at which timepoint, one-way analysis of variance revealed a significant difference in the number of detergent-insoluble EGFP-positive particles per 100 cells across examined genotype groups ($p = 0.0004$, Figure 5C), with significantly more detergent-insoluble ataxin-3 positive particles in dissociated zebrafish expressing EGFP ataxin-3-84Q compared to non-transgenic siblings ($p = 0.0012$) and EGFP ataxin-3 23Q larvae ($p = 0.0009$). Interestingly, use of calibrated microspheres revealed that the size of the detergent-insoluble particles was similar across the genotypes and consistent with aggregate diameters found in other *in vivo* models of SCA3 [41] and SCA3 patient brain tissue [42] (Figure 5D).

We also examined aggregate number and size at 6 dpf, an age at which the 84Q transgenic zebrafish present with a swimming phenotype characterised by reduced distance swum [32]. Again, we found similar numbers of nuclei were detected within 6 dpf samples (p = 0.861, Figure 5E). We also found that the number of detergent-insoluble ataxin-3 aggregates was consistent at both timepoints examined, with a significant difference across genotype groups still evident at 6 dpf (p = 0.0134). Post-hoc analysis revealed that significantly more detergent-insoluble EGFP-positive particles were present in dissociated zebrafish expressing EGFP ataxin-3-84Q compared to non-transgenic siblings (p = 0.0214) and EGFP ataxin-3-23Q-expressing transgenic fish (p = 0.0343, Figure 5F). The size of detergent-insoluble EGFP-positive particles was again found to be similar across analysed genotypes, with mean detergent-insoluble particle diameter around 3 microns in diameter by 6 dpf (Figure 5G).

As proof of the utility of the FloIT approach to assess efficacy of drug treatments aimed at modifying protein aggregate formation and detergent-insoluble protein species, EGFP-ataxin-3 84Q larvae were treated with 3 mM chloroquine, an autophagy inhibitor for 24 hours. A 1.5-fold increase in detergent-insoluble EGFP particles was observed in chloroquine treated larvae compared to vehicle control larvae from the same clutch (p = 0.012, Figure 5H). FloIT also detected a difference in the number of detergent-insoluble EGFP positive particles present following 24-hour treatment with the autophagy inducer calpeptin (p = 0.006, Figure 5I). Post-hoc comparisons revealed that treatment with 25 µM calpeptin produced a statistically significant decrease in detergent-insoluble particles when compared to vehicle treatment (p = 0.038). Treatment with 50 and 100 µM doses appeared to produce a decrease in detergent-insoluble particles, however these comparisons were not statistically significant (p = 0.055 and p = 0.053, respectively).

Discussion

Flow cytometry approach detects protein aggregates in a cell culture model of SCA3

Here we report that neuronal-like (neuroblastoma) SH-SY5Y cells expressing EGFP-ataxin-3 containing a polyQ expansion (84 polyQ repeats) develop EGFP-positive protein aggregates. These findings align with existing experimental evidence that suggests polyglutamine expanded ataxin-3 can form protein aggregates within cultured murine or

human neuroblastoma cells [11, 41, 43, 44]. Interestingly, we observed ataxin-3 protein aggregates predominately in the cell cytoplasm, contrasting with reports of intranuclear ataxin-3 positive inclusions in SCA3 brain tissue [11, 13, 42, 45]. Our findings of predominately cytoplasmic ataxin-3 protein aggregates are consistent with existing evidence of cytoplasmic protein aggregates in cultured cells transiently expressing a EGFP fused to the N-terminus of the human ataxin-3 protein with 84 polyglutamines [44, 46-51]. In contrast, experiments involved mutant expanded ataxin-3 with EGFP fused to the C-terminus display predominately nuclear ataxin-3 aggregates [52]. As such, the location of the fused fluorescent protein may alter the localisation of observed protein aggregates.

In addition to examining protein aggregation in our cell culture and transgenic zebrafish models of SCA3, we also utilised western blotting to examine the expression of ataxin-3 across our models. The purpose of our western blotting experiments was to confirm that the increased presence of EGFP ataxin-3 aggregates in our models expressing mutant expanded ataxin-3 was not due to underlying differences in protein expression. In our cell cultures, we found the expression of ataxin-3 to be significantly higher in cells transiently expressing EGFP-fused ataxin-3 with 28Q compared to cells transiently expressing EGFP-fused ataxin-3 with 84Q. In our transgenic zebrafish, expression of human ataxin-3 was found to be similar across larvae expressing EGFP ataxin-3 23Q and EGFP ataxin-3 84Q, however transgene expression may vary across different clutches of zebrafish embryos. This suggests that the increased presence of ataxin-3 positive protein aggregates in SCA3 cells and transgenic zebrafish is not a consequence of underlying differences in the expression of the ataxin-3 protein, but likely due pathological expansion of the polyQ region within the ataxin-3 protein, as previously reported [53-56].

Next, we aimed to determine if we could employ the high-throughput flow cytometric analysis approach, FloIT [20], to quantify the number and size of detergent-insoluble ataxin-3 particles in SCA3 cells. This method has been previously utilized to quantify TDP-43, SOD1 and huntingtin-positive inclusions [20-22] and other cellular processes associated with protein aggregation, including heatshock response induction [24], the role of

molecular chaperones in suppressing protein aggregation [25] and chaperone assisted selective autophagy [26]. Here we provide the first adaption of FloIT to examine the presence of detergent-insoluble protein species in a model of Spinocerebellar Ataxia. FloIT analysis revealed the presence of more Triton-X insoluble EGFP-positive aggregates in cells expressing EGFP-ataxin-3 84Q than those expressing EGFP-ataxin-3 28Q or EGFP controls. This finding is consistent with existing reports that utilise western blotting and filter trap assays to provide evidence of detergent-insoluble forms of ataxin-3 in cell culture models expressing mutant expanded ataxin-3 fused to GFP [46, 50, 52].

In the present study, we utilised microscopy to determine the transfection efficiency in our cell culture models. This approach contrasts with previous publications that have utilised FloIT, where flow cytometry was used to determine the transfection efficiency [20-24]. It is possible that quantification of the proportion of transfected cells using microscopy may yield a lower detection threshold than more sensitive flow cytometry methods, resulting in a lower reported transfection efficiency. As transfection efficiency is incorporated into the FloIT equation, decreased transfection efficiency could decrease the denominator in the FloIT equation and thus alter the total number of insoluble particles per 100 transfected nuclei detected. Therefore, when utilising FloIT it is important to consider how the different methodological approaches used to calculate transfection efficiency could alter the overall number of insoluble particles per nuclei detected. It is recommended that future experiments remain consistent in the approach employed as inconsistency in calculation of transfection efficiency could introduce variability.

Our flow cytometry findings are supported by existing reports of ataxin-3 aggregate formation and size, aligning with findings from Weishäupl et al [52] that demonstrated that cultured cells transiently transfected with human ataxin-3 constructs develop ataxin-3 positive aggregates within 24 hours. Interestingly, Weishäupl et al [52] did not detect a significant difference in the number of aggregates present at 24-hours post transfection in cells expressing ataxin-3 with a short polyQ chain and cells expressing ataxin-3 with a long

polyQ chain, conflicting with the present findings. However, Weishäupl et al [52] investigated ataxin-3 proteinopathy in an immortal human embryonic kidney cell line, whilst the present study utilised human neuronal-like (neuroblastoma) SHSY5Y cells. It is possible that these different cell lines may possess different intrinsic susceptibilities to aggregate formation. Additionally, it is possible that differences in protein expression could alter the amount of proteinopathy present [57, 58]. Indeed, gene expression may also influence the formation of protein aggregates in cell culture models [58]. Furthermore, contrasting methodological approaches were employed, with Weishäupl and colleagues using microscopy to visualise and quantify ataxin-3 proteinopathy and microscopy approaches may lack the sensitivity required to detect ataxin-3 aggregates at this time point.

Transgenic zebrafish expressing mutant ataxin-3 develop protein aggregates from two days of age

Here we provide the first adaption of FloIT for use with an *in vivo* model. We were able to successfully quantify the number of Triton-X insoluble EGFP-positive protein aggregates present within our transgenic zebrafish model of SCA3 that express EGFP fused to human ataxin-3 under a neuronal promotor (HuC, elavl3). We found that our transgenic zebrafish expressing EGFP-fused to human ataxin-3 containing a long polyQ stretch (84 glutamine residues) displayed significantly more detergent-insoluble EGFP-ataxin-3 inclusions than non-transgenic siblings or zebrafish expressing ataxin-3 with a short polyQ stretch fused to EGFP (23 glutamine residues). Interestingly, this phenotype was detectable at two different time points in SCA3 zebrafish development; two days post-fertilisation, prior to the onset of swimming deficits, and six days post-fertilisation, when a movement phenotype is detectable [32]. This suggests that formation of detergent-insoluble ataxin-3 aggregates may be an early disease phenotype that may contribute to the development of neurotoxicity, neurodegeneration and motor impairment. Further, we found that treatment with a compound that we have previously demonstrated to improve swimming of these zebrafish (calpeptin), does indeed also decrease the presence of this insoluble protein [32].

The ability to detect the presence of this protein aggregation phenotype at such an early timepoint, including the larval stages, has many advantages. Firstly, FloIT is a relatively inexpensive and efficient analysis tool that can be utilised to provide a rapid readout of treatment efficacy on protein aggregation in cells dissociated from large clutches of sibling zebrafish larvae. We suggest that using FloIT to examine proteinopathy phenotypes may be valuable within high-throughput drug screening pipeline in zebrafish models of proteinopathy and neurodegenerative diseases, either on its own, or together with tracking of locomotion behaviour (Figure 4). Zebrafish larvae can be assayed for improvements in swimming and then dissociated into single cells at the completion of the experiment, enabling identification of compounds that induce beneficial effects on animal movement and cellular phenotypes. At these early larval stages drugs and small compounds can easily be dissolved in the water that the larvae are incubated within, and are absorbed by the larvae, making dosing straight-forward [33]. Further, in comparison with more traditional methodologies for detecting proteinopathy, such as western blotting, live imaging confocal microscopy and immunostaining, this flow cytometry approach is much less time consuming and laborious. Whilst these other methodologies may provide critical insights relating to the relative expression and location of ataxin-3 positive inclusions, these approaches can also be incorporated into a possible drug testing workflow for greatest insight.

To validate the use of this FloIT approach to investigate potential treatments of SCA3, and related diseases, and to confirm that the detected particles are indeed protein aggregates, we examined the effect of treatment with autophagy modifying compounds on the number of particles detected. We hypothesised that treatment with autophagy inhibitors, 3MA *in vitro* or chloroquine *in vivo*, would result in an increase in the number of insoluble EGFP-ataxin-3 aggregates due to blockage of their removal. Further, we hypothesised that treatment with calpeptin, a compound known to inhibit activity of calpain proteases and induce autophagic activity, would decrease the number of detergent-insoluble EGFP-ataxin-3 aggregates present. Indeed, we found that treating SHSY5Y cells or zebrafish expressing EGFP-ataxin-3 84Q with autophagy inhibitor compounds increased the number of detergent-insoluble EGFP-ataxin-3 aggregates detected by FloIT. In contrast, treatment with calpeptin reduced detergent-insoluble ataxin-3 particles in both cell culture and zebrafish models of SCA3. Our *in vitro* findings support existing work by Haacke et al [38], providing further evidence that treatment with low doses of calpeptin can decrease presence of detergent-insoluble ataxin-3 protein aggregates in cell culture models of SCA3. Further, our zebrafish findings build upon our previous reports that calpeptin can increase activity of the autophagy protein quality

control pathway [32] in SCA3 zebrafish. These findings confirm that the FloIT approach can be used to examine the effect of autophagy modulators and validates the approach for quantification of ataxin-3 aggregates. If the approach were detecting random debris proteins or undigested whole cells, the observed fluctuations in total detergent-insoluble protein species would not have been affected by administration of autophagy modifying compounds.

One caveat of this approach is that the FloIT protocol requires expression of the protein of interest fused to a fluorescent protein. Attachment of a fusion protein has the potential to alter protein dynamics or conformation, potentially rendering the protein more aggregation-prone than endogenous or native forms of the protein [59]. However, within this study, EGFP-fused mutant ataxin-3 proteins was directly compared against EGFP-fused wild type ataxin-3 protein, meaning that any the increase in detergent-insoluble protein species can be attributed to the presence of the expanded polyQ stretch within the ataxin-3 protein, not the fused fluorescent protein itself. Further, we have previously found in a separate series of experiments that SHSY5Y cells stably expressing human ataxin-3 with 28 or 84 glutamines develop ataxin-3 positive protein aggregates when in absence of EGFP fusion [60]. Additionally, we have also considered whether fusion of EGFP to human ataxin-3 may contribute to the swimming phenotypes observed in our transgenic zebrafish and have found that transgenic zebrafish expressing human ataxin-3 (not fused to a fluorescent protein) under the same neuronal promoter also develop abnormal swimming phenotypes by 6 dpf (data not shown). These findings suggests that the protein aggregation phenotypes described in the present study are not caused by fusion of EGFP to ataxin-3, but likely caused by expansion of the polyQ region within the ataxin-3 protein. It is important to conduct similar control experiments within future studies utilizing the FloIT approach to ensure that fusion of a fluorescent protein does not increase the aggregation propensity of the studied protein of interest.

The FloIT methodology is one of many recent flow cytometric methodology developed to investigate protein aggregation in cultured cells expressing aggregation-prone proteins fused to fluorescent proteins. Other approaches include PulSA, a flow cytometric approach that allows identification of intact cells containing protein inclusions or aggregates. PulSA can be used to identify cellular populations containing protein inclusions or aggregates based on differences in cell size and shape (pulse width and height) [61]. Similarly, cultured cells can be lysed with 0.03% saponin allowing diffusion of soluble proteins into the extracellular space and trapping insoluble proteins (and fused fluorescent proteins) within the cell [62]. However, PulSA has been found to be ineffective at identifying cells with a low number of

inclusions or aggregates per cell and may be more suited to identifying cells containing many aggregates/inclusions per cell [20]. For this reason, FloIT may be more suitable for the rapid quantification of protein aggregates in cell populations where many cells harbour sparse (1-3) protein aggregates. Further, PulSA or saponin approaches provide an estimation of the number of cells within a population affected by protein inclusions or aggregates, however as FloIT lyses cell membranes this type of information cannot be obtained from this approach. Researchers should consider which approach may be most suited to their experimental aims before embarking on flow cytometric analysis of proteinopathy.

In conclusion, our findings highlight the utility of FloIT as a rapid approach to quantify protein aggregation, which can be utilised to screen novel compounds *in vitro* and *in vivo*. We report this novel approach of applying FloIT to transgenic zebrafish samples that can be incorporated into a drug testing pipeline to aid identification of compounds that slow or prevent disease progression including ameliorating protein aggregation and swimming impairment.

Ethics Approval:

All animal experiments were performed in accordance with the Code and approved by the Animal Ethics Committee of Macquarie University (2016/004 and 2017/019).

Consent for Publication:

Not applicable

Availability of Data and Materials:

The datasets used in the current study are available from the corresponding author on reasonable request.

Competing Interests:

The authors declare that they have no competing interests.

Funding:

This work was funded by: MJD Foundation, Australia; Australian National Health and Medical Research Council (Project Grant 1069235 and 1146750); The Snow Foundation, Australia; Motor Neuron Disease Research Australia; Macquarie University DVCR Start-up Funding and Research Development Grant. The Swedish SCA Network also provided donation support for this work. KJR is supported by a Macquarie University MQRES scholarship.

Author Contributions:

KJR and ASL conceptualized the study. KJR performed the cell culture and zebrafish studies, data analysis, interpretation, and manuscript preparation. MCT and AH assisted in developing the methodological approach. AH, KCY, SP and MW assisted with performing experiments. EKD assisted with experimental design, interpretation of findings and project supervision. ASL provided project supervision, performed data analysis, interpretation, and manuscript preparation. All authors have read and agreed to the published version of the manuscript.

Acknowledgments:

The authors would like to acknowledge Dr Elena Shklovskaya and Miss Bernadette Pederson for providing technical support and analysis advice for flow cytometry experiments. Figure 4 was created using Biorender.com.

References

1. Costa Mdo, C. and H.L. Paulson, *Toward understanding Machado-Joseph disease.* Prog Neurobiol, 2012. **97**(2): p. 239-57.
2. Dürr, A., et al., *Spinocerebellar ataxia 3 and Machado-Joseph disease: clinical, molecular, and neuropathological features.* Ann Neurol, 1996. **39**(4): p. 490-9.
3. Ranum, L.P., et al., *Spinocerebellar ataxia type 1 and Machado-Joseph disease: incidence of CAG expansions among adult-onset ataxia patients from 311 families with dominant, recessive, or sporadic ataxia.* Am J Hum Genet, 1995. **57**(3): p. 603-8.

4. Schöls, L., et al., *Trinucleotide expansion within the MJD1 gene presents clinically as spinocerebellar ataxia and occurs most frequently in German SCA patients.* Hum Mol Genet, 1995. **4**(6): p. 1001-5.

5. Kawaguchi, Y., et al., *CAG expansions in a novel gene for Machado-Joseph disease at chromosome 14q32.1.* Nat Genet, 1994. **8**(3): p. 221-8.

6. Takiyama, Y., et al., *The gene for Machado-Joseph disease maps to human chromosome 14q.* Nat Genet, 1993. **4**(3): p. 300-4.

7. Maciel, P., et al., *Correlation between CAG repeat length and clinical features in Machado-Joseph disease.* American journal of human genetics, 1995. **57**(1): p. 54-61.

8. Jardim, L.B., et al., *Neurologic Findings in Machado-Joseph Disease: Relation With Disease Duration, Subtypes, and (CAG)n.* Archives of Neurology, 2001. **58**(6): p. 899-904.

9. Abe, Y., et al., *CAG repeat number correlates with the rate of brainstem and cerebellar atrophy in Machado-Joseph disease.* Neurology, 1998. **51**(3): p. 882.

10. Kieling, C., et al., *Survival estimates for patients with Machado–Joseph disease (SCA3).* Clinical Genetics, 2007. **72**(6): p. 543-545.

11. Schmidt, T.L., B.; Schmitt, I.; Trottier, Y.; Auburger, G.; Laccone, F.; Klockgether, T.; Volpel, M.; Epplen, J.T.; Schols, L.; Riess, O., *An isoform of ataxin-3 accumulates in the nucleus of neuronal cells in affected brain regions of SCA3 patients.* Brain Pathology, 1998. **8**: p. 669-679.

12. Rüb, U., et al., *Clinical features, neurogenetics and neuropathology of the polyglutamine spinocerebellar ataxias type 1, 2, 3, 6 and 7.* Prog Neurobiol, 2013. **104**: p. 38-66.

13. Yamada, M.T., S.; Takahashi, H., *Pathology of CAG repeat diseases.* Neuropathology, 2000. **20**: p. 319-325.

14. Scheel, H., S. Tomiuk, and K. Hofmann, *Elucidation of ataxin-3 and ataxin-7 function by integrative bioinformatics.* Hum Mol Genet, 2003. **12**(21): p. 2845-52.

15. Yang, H., et al., *Aggregation of polyglutamine-expanded ataxin-3 sequesters its specific interacting partners into inclusions: Implication in a loss-of-function pathology.* Scientific Reports, 2014. **4**(1): p. 6410.

16. Donaldson, K.M., et al., *Ubiquitin-mediated sequestration of normal cellular proteins into polyglutamine aggregates.* Proceedings of the National Academy of Sciences, 2003. **100**(15): p. 8892.

17. Gusella, J.F. and M.E. MacDonald, *Molecular genetics: Unmasking polyglutamine triggers in neurodegenerative disease.* Nature Reviews Neuroscience, 2000. **1**(2): p. 109-115.

18. Hands, S.L. and A. Wyttenbach, *Neurotoxic protein oligomerisation associated with polyglutamine diseases.* Acta Neuropathologica, 2010. **120**(4): p. 419-437.

19. Rubinsztein, D.C., C.F. Bento, and V. Deretic, *Therapeutic targeting of autophagy in neurodegenerative and infectious diseases.* J Exp Med, 2015. **212**(7): p. 979-90.

20. Whiten, D.R., et al., *Rapid flow cytometric measurement of protein inclusions and nuclear trafficking.* Scientific Reports, 2016. **6**(1): p. 31138.

21. McAlary, L., J.A. Aquilina, and J.J. Yerbury, *Susceptibility of Mutant SOD1 to Form a Destabilized Monomer Predicts Cellular Aggregation and Toxicity but Not In vitro Aggregation Propensity.* Frontiers in Neuroscience, 2016. **10**(499).

22. Zeineddine, R., et al., *Flow cytometric measurement of the cellular propagation of TDP-43 aggregation.* Prion, 2017. **11**(3): p. 195-204.

23. Zeineddine, R., et al., *Addition of exogenous SOD1 aggregates causes TDP-43 mislocalisation and aggregation.* Cell Stress and Chaperones, 2017. **22**(6): p. 893-902.

24. San Gil, R., et al., *Neurodegenerative disease-associated protein aggregates are poor inducers of the heat shock response in neuronal cells.* J Cell Sci, 2020. **133**(15).

25. McMahon, S., et al., *DNAJB chaperones suppress destabilised protein aggregation via a region distinct from that used to inhibit amyloidogenesis.* Journal of Cell Science, 2021. **134**(7).

26. Adriaenssens, E., et al., *BAG3 Pro209 mutants associated with myopathy and neuropathy relocate chaperones of the CASA-complex to aggresomes.* Scientific Reports, 2020. **10**(1): p. 8755.

27. Chiti, F. and C.M. Dobson, *Protein Misfolding, Amyloid Formation, and Human Disease: A Summary of Progress Over the Last Decade.* Annual Review of Biochemistry, 2017. **86**(1): p. 27-68.

28. Ross, C.A. and M.A. Poirier, *Protein aggregation and neurodegenerative disease.* Nature Medicine, 2004. **10**(7): p. S10-S17.

29. Taylor, J.P., J. Hardy, and K.H. Fischbeck, *Toxic Proteins in Neurodegenerative Disease.* Science, 2002. **296**(5575): p. 1991.

30. Gidalevitz, T., et al., *Progressive Disruption of Cellular Protein Folding in Models of Polyglutamine Diseases.* Science, 2006. **311**(5766): p. 1471.

31. Mukherjee, A., et al., *Type 2 diabetes as a protein misfolding disease.* Trends in Molecular Medicine, 2015. **21**(7): p. 439-449.

32. Watchon, M., et al., *Calpain Inhibition Is Protective in Machado-Joseph Disease Zebrafish Due to Induction of Autophagy.* The Journal of neuroscience : the official journal of the Society for Neuroscience, 2017. **37**(32): p. 7782-7794.

33. Zon, L.I. and R.T. Peterson, *In vivo drug discovery in the zebrafish.* Nature Reviews Drug Discovery, 2005. **4**(1): p. 35-44.

34. Schneider, C.A., W.S. Rasband, and K.W. Eliceiri, *NIH Image to ImageJ: 25 years of image analysis.* Nature Methods, 2012. **9**(7): p. 671-675.

35. Acosta, J.R., et al., *Neuronal cell culture from transgenic zebrafish models of neurodegenerative disease.* Biology Open, 2018. **7**(10).

36. Klionsky, D.J., et al., *Guidelines for the use and interpretation of assays for monitoring autophagy (4th edition).* Autophagy, 2021: p. 1-382.

37. Williams, A., et al., *Novel targets for Huntington's disease in an mTOR-independent autophagy pathway.* Nat Chem Biol, 2008. **4**(5): p. 295-305.

38. Haacke, A., F.U. Hartl, and P. Breuer, *Calpain inhibition is sufficient to suppress aggregation of polyglutamine-expanded ataxin-3.* J Biol Chem, 2007. **282**(26): p. 18851-6.

39. Seglen, P.O. and P.B. Gordon, *3-Methyladenine: specific inhibitor of autophagic/lysosomal protein degradation in isolated rat hepatocytes.* Proc Natl Acad Sci U S A, 1982. **79**(6): p. 1889-92.

40. Menzies, F.M., et al., *Calpain inhibition mediates autophagy-dependent protection against polyglutamine toxicity.* Cell death and differentiation, 2015. **22**(3): p. 433-444.

41. Santana, M.M., et al., *Trehalose alleviates the phenotype of Machado–Joseph disease mouse models.* Journal of Translational Medicine, 2020. **18**(1): p. 161.

42. Paulson, H.L., et al., *Intranuclear inclusions of expanded polyglutamine protein in spinocerebellar ataxia type 3.* Neuron, 1997. **19**(2): p. 333-44.

43. Yoshizawa, T., H. Yoshida, and S.i. Shoji, *Differential susceptibility of cultured cell lines to aggregate formation and cell death produced by the truncated Machado-Joseph disease gene product with an expanded polyglutamine stretch.* Brain Research Bulletin, 2001. **56**(3): p. 349-352.

44. van Well, E.M., et al., *A protein quality control pathway regulated by linear ubiquitination.* The EMBO Journal, 2019. **38**(9): p. e100730.

45. Rüb, U., E.R. Brunt, and T. Deller, *New insights into the pathoanatomy of spinocerebellar ataxia type 3 (Machado–Joseph disease).* Current Opinion in Neurology, 2008. **21**(2): p. 111-116.

46. Joshi, V., et al., *Polyphenolic flavonoid (Myricetin) upregulated proteasomal degradation mechanisms: Eliminates neurodegenerative proteins aggregation.* Journal of Cellular Physiology, 2019. **234**(11): p. 20900-20914.

47. Pavel, M., et al., *CCT complex restricts neuropathogenic protein aggregation via autophagy.* Nature Communications, 2016. **7**(1): p. 13821.

48. Khan, E., et al., *Discovery of a potent small molecule inhibiting Huntington's disease (HD) pathogenesis via targeting CAG repeats RNA and Poly Q protein.* Scientific Reports, 2019. **9**(1): p. 16872.

49. Rajamani, K., et al., *n-Butylidenephthalide exhibits protection against neurotoxicity through regulation of tryptophan 2, 3 dioxygenase in spinocerebellar ataxia type 3.* Neuropharmacology, 2017. **117**: p. 434-446.

50. Chang, K.-H., et al., *Aqueous extract of Gardenia jasminoides targeting oxidative stress to reduce polyQ aggregation in cell models of spinocerebellar ataxia 3.* Neuropharmacology, 2014. **81**: p. 166-175.

51. Upadhyay, A., et al., *Lanosterol Suppresses the Aggregation and Cytotoxicity of Misfolded Proteins Linked with Neurodegenerative Diseases.* Molecular Neurobiology, 2018. **55**(2): p. 1169-1182.

52. Weishäupl, D., et al., *Physiological and pathophysiological characteristics of ataxin-3 isoforms.* Journal of Biological Chemistry, 2018.

53. Haacke, A., et al., *Proteolytic cleavage of polyglutamine-expanded ataxin-3 is critical for aggregation and sequestration of non-expanded ataxin-3.* Human Molecular Genetics, 2006. **15**(4): p. 555-568.

54. Evers, M.M., L.J.A. Toonen, and W.M.C. van Roon-Mom, *Ataxin-3 protein and RNA toxicity in spinocerebellar ataxia type 3: current insights and emerging therapeutic strategies.* Molecular neurobiology, 2014. **49**(3): p. 1513-1531.

55. Ellisdon, A.M., B. Thomas, and S.P. Bottomley, *The Two-stage Pathway of Ataxin-3 Fibrillogenesis Involves a Polyglutamine-independent Step*.* Journal of Biological Chemistry, 2006. **281**(25): p. 16888-16896.

56. Bevivino, A.E. and P.J. Loll, *An expanded glutamine repeat destabilizes native ataxin-3 structure and mediates formation of parallel β-fibrils.* Proceedings of the National Academy of Sciences, 2001. **98**(21): p. 11955-11960.

57. Kiefhaber, T., et al., *Protein Aggregation in vitro and in vivo: A Quantitative Model of the Kinetic Competition between Folding and Aggregation.* Bio/Technology, 1991. **9**(9): p. 825-829.

58. Tartaglia, G.G., et al., *Life on the edge: a link between gene expression levels and aggregation rates of human proteins.* Trends Biochem Sci, 2007. **32**(5): p. 204-6.

59. Snapp, E., *Design and use of fluorescent fusion proteins in cell biology.* Current protocols in cell biology, 2005. **Chapter 21**: p. 21.4.1-21.4.13.

60. Watchon, M., et al., *Treatment with sodium butyrate has therapeutic benefits for Machado-Joseph disease through the induction of autophagy.* bioRxiv, 2021: p. 2021.04.30.442119.

61. Ramdzan, Y.M., et al., *Tracking protein aggregation and mislocalization in cells with flow cytometry.* Nature Methods, 2012. **9**(5): p. 467-470.

62. Pokrishevsky, E., et al., *Tryptophan 32-mediated SOD1 aggregation is attenuated by pyrimidine-like compounds in living cells.* Scientific Reports, 2018. **8**(1): p. 15590.

Figures

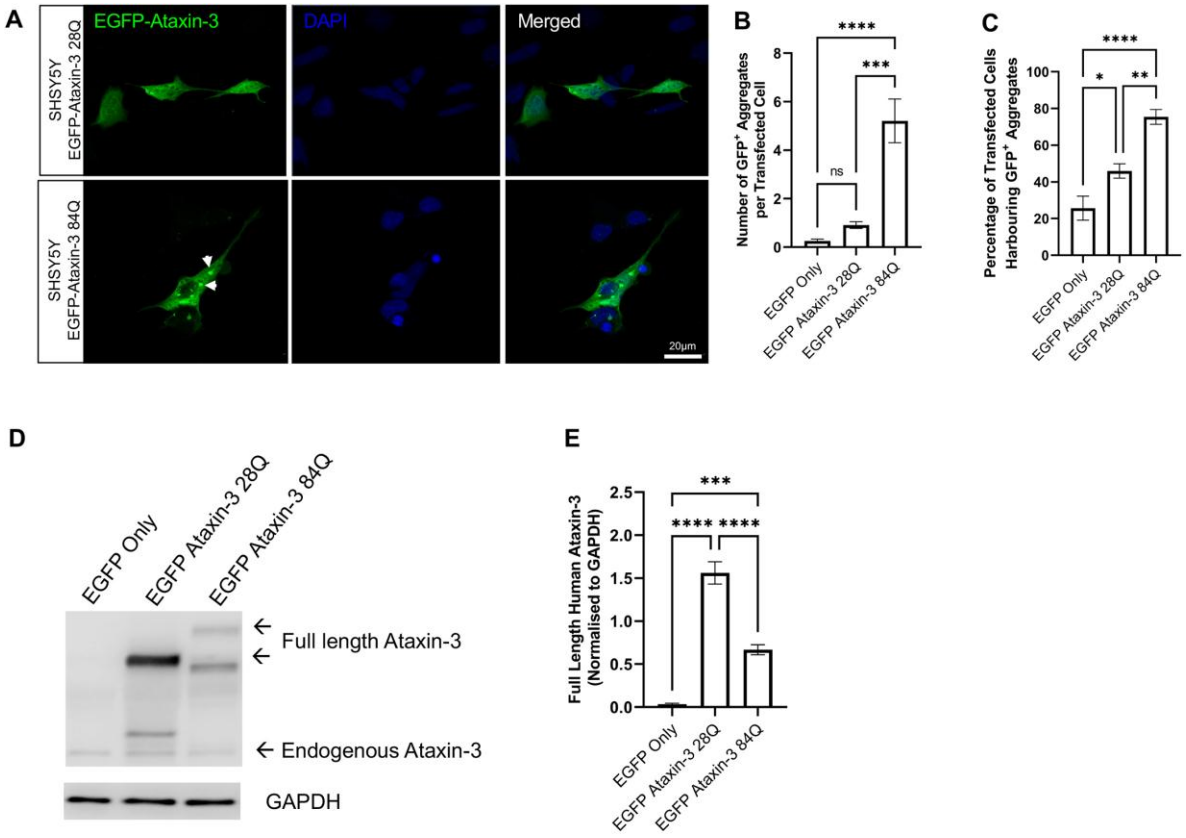

Figure 1. Neuronal-like SHSY5Y cells develop EGFP ataxin-3 protein aggregates. (A) SHSY5Y cells transiently expressing EGFP-fused human ataxin-3 develop protein aggregates. (B) The mean number of aggregates per transfected cell was calculated by averaging six experimental replicates (different fields of view) per coverslip. Aggregates were more commonly observed in cells transfected with the 84Q repeat expansion than cells transfected with ataxin-3 28Q. (C) Quantification of the percentage of cells harbouring protein aggregates revealed significantly more cells were affected by protein aggregates following transient transfection with EGFP ataxin-3 84Q when compared to EGFP ataxin-3 28Q or EGFP only. (D) Western blotting was used to examine the expression of ataxin-3 following transient transfection of EGFP constructs. (E) Expression of EGFP-fused ataxin-3 was found to be significantly higher in cells transfected with EGFP only or EGFP ataxin-3 84Q. * indicates $p < 0.05$, ** indicates $p < 0.01$, *** indicates $p < 0.001$ and **** indicates $p < 0.0001$. Graphs depict mean ± standard error mean, n = 4-5 experimental replicates.

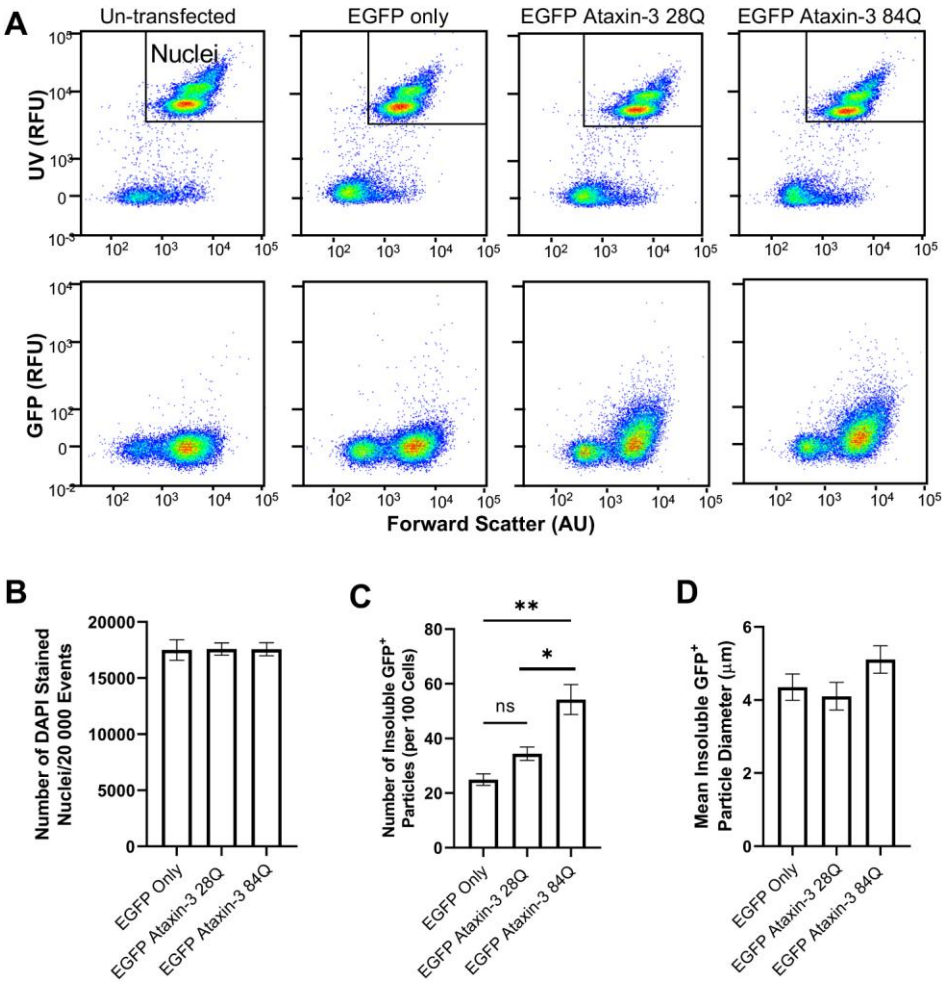

Figure 2. Flow cytometry can be used to quantify the number of detergent-insoluble EGFP ataxin-3 particles relative to the number of nuclei. (A) Representative flow cytometry scatterplots displaying UV-positive nuclei and EGFP-fused ataxin-3 particles from cell lysates. (B) Quantification of the number of DAPI-positive nuclei revealed similar numbers of nuclei were present in analysed samples. (C) Cells expressing EGFP-fused mutant ataxin-3 (84Q glutamines) develop significantly more insoluble particles when compared to EGFP alone or EGFP-fused ataxin-3 with a short polyglutamine stretch (28 glutamines). (D) Detergent-insoluble particle size did not significantly differ across examined genotypes. * indicates $p < 0.05$ and ** indicates $p < 0.01$, *** indicates $p < 0.001$ and **** indicates $p < 0.0001$. Graphs depict mean ± standard error mean, n = 4-9 experimental replicates.

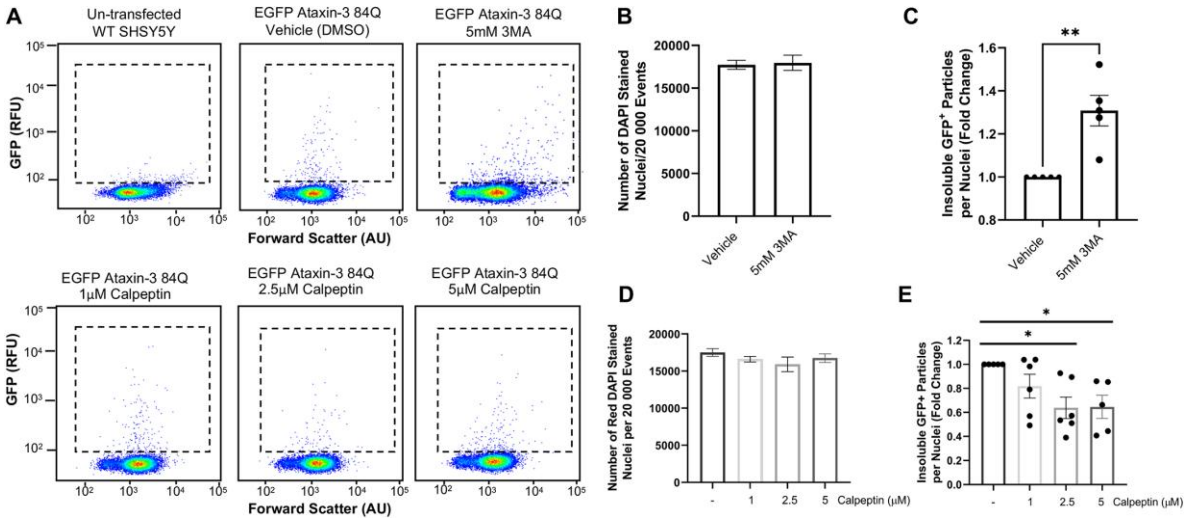

Figure 3. Treatment with autophagy pathway modulators altered the number of EGFP-fused particles present in cells expressing human ataxin-3 with 84 glutamines. (A) Representative scatterplots reveal a scarcity of EGFP-fused particles in un-transfected control cells and altered numbers of particles following treatment with autophagy modulators (3MA and calpeptin). (B) Quantification of the number of DAPI-positive nuclei reveal a similar number of nuclei were present across vehicle treated and 3MA treated samples. (C) Comparison of cells treated with vehicle or 3MA (5 mM) revealed a statistically significant increase in detergent-insoluble particles relative to the number of nuclei following 3MA treatment. (D) Similar numbers of nuclei were quantified in samples treated with a vehicle control or calpeptin. (E) Calpeptin treatment produced reductions in detergent-insoluble particles as detected by FloIT . * indicates $p < 0.05$, ** indicates $p < 0.01$. Graphs depict mean ± standard error mean, n = 2-6 experimental replicates.

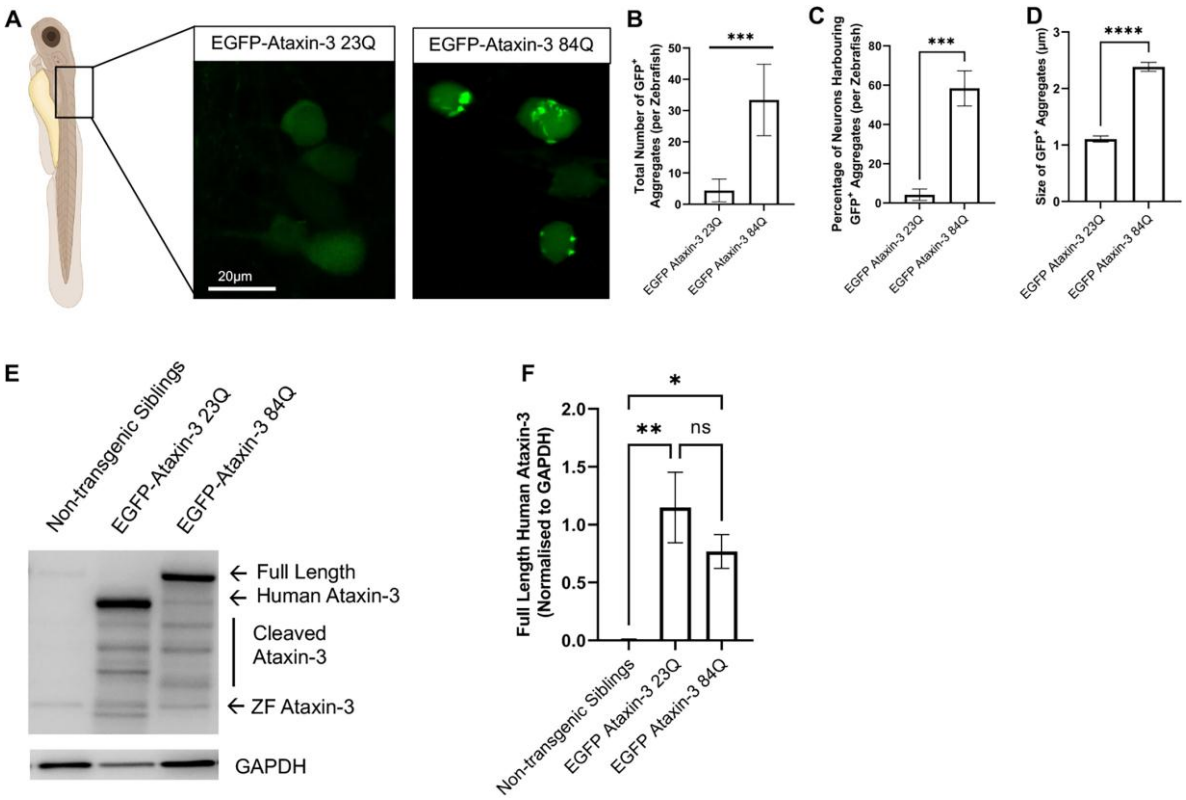

Figure 4. Transgenic zebrafish expressing human ataxin-3 with 84 glutamines develop ataxin-3 positive protein aggregates (A) Confocal microscopy was performed on 6-day old zebrafish larvae expressing EGFP- tagged human ataxin-3 containing a short polyglutamine stretch (28Q) or long polyglutamine stretch (84Q). (B) Manual counting of EGFP aggregates revealed that significantly more aggregates were present in 6 dpf zebrafish expressing EGFP-ataxin-3 84Q then EGFP-ataxin-3 23Q. (C) Quantification of the percentage of cells harbouring protein aggregates revealed a greater number of cells were affected with aggregates in zebrafish expressing EGFP ataxin-3 84Q. (D) Measurement of the size of protein aggregates observed via confocal microscopy revealed that zebrafish expressing EGFP ataxin-3 84Q also display aggregates that are significantly larger in size when compared to the aggregates found in zebrafish expressing EGFP ataxin-3 23Q. (E) Western blotting was used to examine the relative expression of human ataxin-3 across examined genotypes. (F) Densiometric analysis revealed significantly greater expression of EGFP-fused human ataxin-3 in transgenic zebrafish when compared to non-transgenic siblings. * indicates $p < 0.05$, ** indicates $p < 0.01$, *** indicates $p < 0.001$, **** indicates $p < 0.0001$. Graphs depict mean ± standard error mean, n = 4-5 experimental replicates.

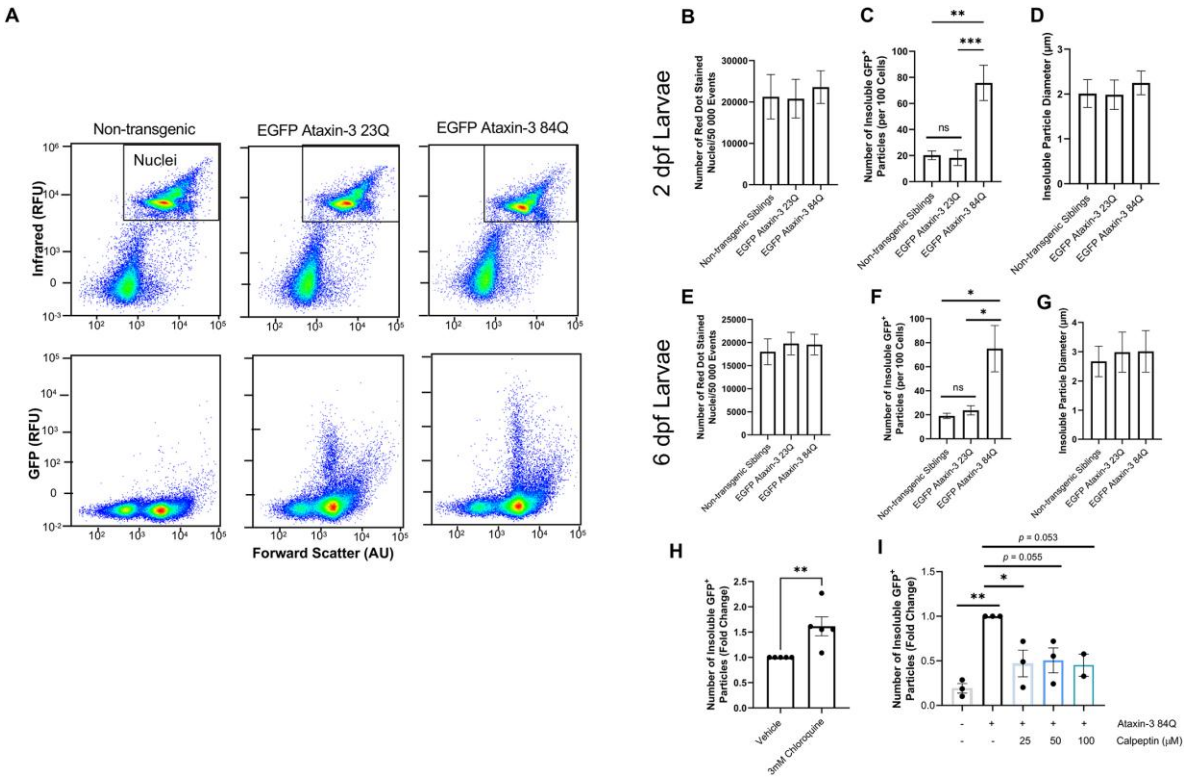

Figure 5. Flow cytometric analysis of dissociated cells from whole zebrafish can be used to rapidly quantify insoluble EGFP ataxin-3 particles and screen compounds for the effect on proteinopathy. (A) Representative scatterplots of flow cytometric populations from dissociated 6-day old zebrafish revealed changes in the number of detected detergent-insoluble particles despite similar numbers of nuclei. (B-C) Zebrafish expressing human mutant ataxin-3 display similar numbers of RedDot^{TM} stained nuclei but significantly more detergent-insoluble ataxin-3 particles at 2 days of age. (D) Examination of insoluble particle size revealed similar sized particles across genotypes. (E-F) At 6 days post-fertilisation, cells from dissociated zebrafish showed similar numbers of nuclei but more EGFP ataxin-3 particles were detected in cells obtained from zebrafish expressing human mutant ataxin-3 when compared to non-transgenic siblings and zebrafish larvae expressing human wildtype ataxin-3. (G) Detergent-insoluble particles were found to be a similar size in cells obtained from zebrafish expressing wildtype human ataxin-3 and mutant human ataxin-3. (H) Treatment with the autophagy inducer calpeptin decreased the number of detergent-insoluble particles detected. (I) Treatment with the autophagy inhibitor chloroquine (3 mM) increased the number of detergent-insoluble particles in 2-day post-fertilisation zebrafish expressing mutant ataxin-3; * indicates $p < 0.05$, ** indicates $p < 0.01$, *** indicates $p < 0.001$. Graphs depict mean ± standard error mean, n = 2-9 experimental replicates.

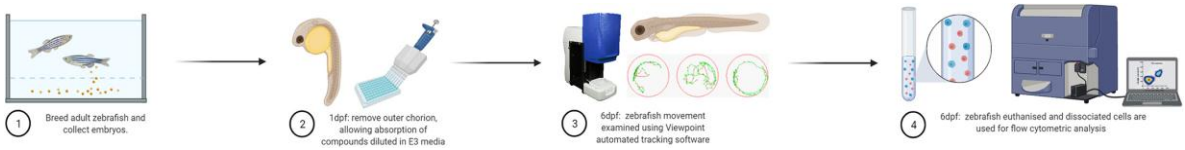

Figure 6. Flow cytometric analysis of cells dissociated from zebrafish larvae can be a powerful addition to high-throughput drug screening pipelines, revealing cellular level insights.

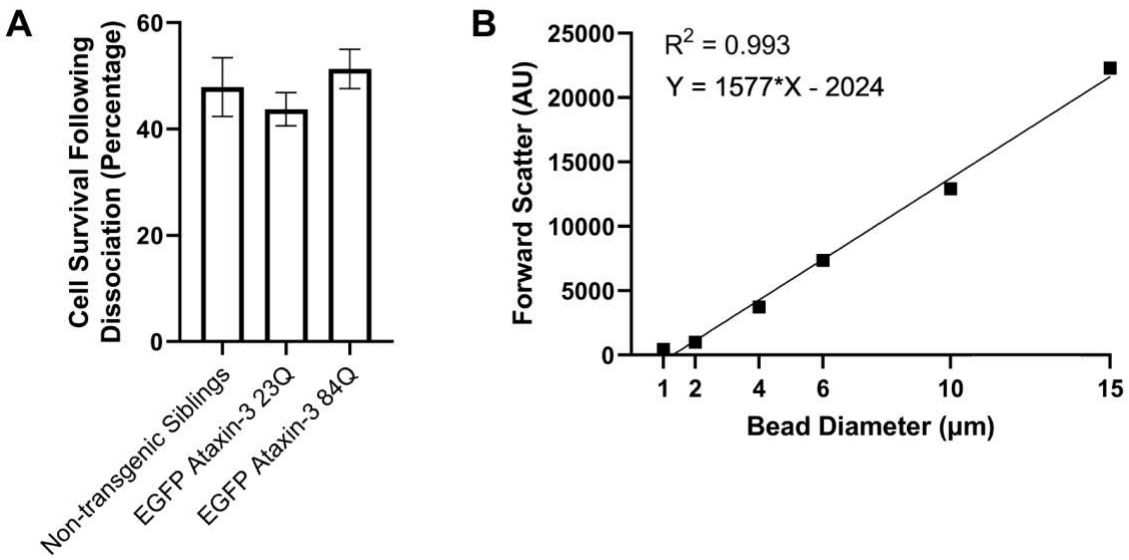

Fig. S1. (A) Staining of cells dissociated from 6 day-old zebrafish revealed greater than 40% of cells were stained with Hoechst live cell stain, suggesting greater than 40% survival post-dissociation. (B) Beads of a known micron diameter were used to calculate the relative size of insoluble GFP-positive particles using the displayed standard curve.

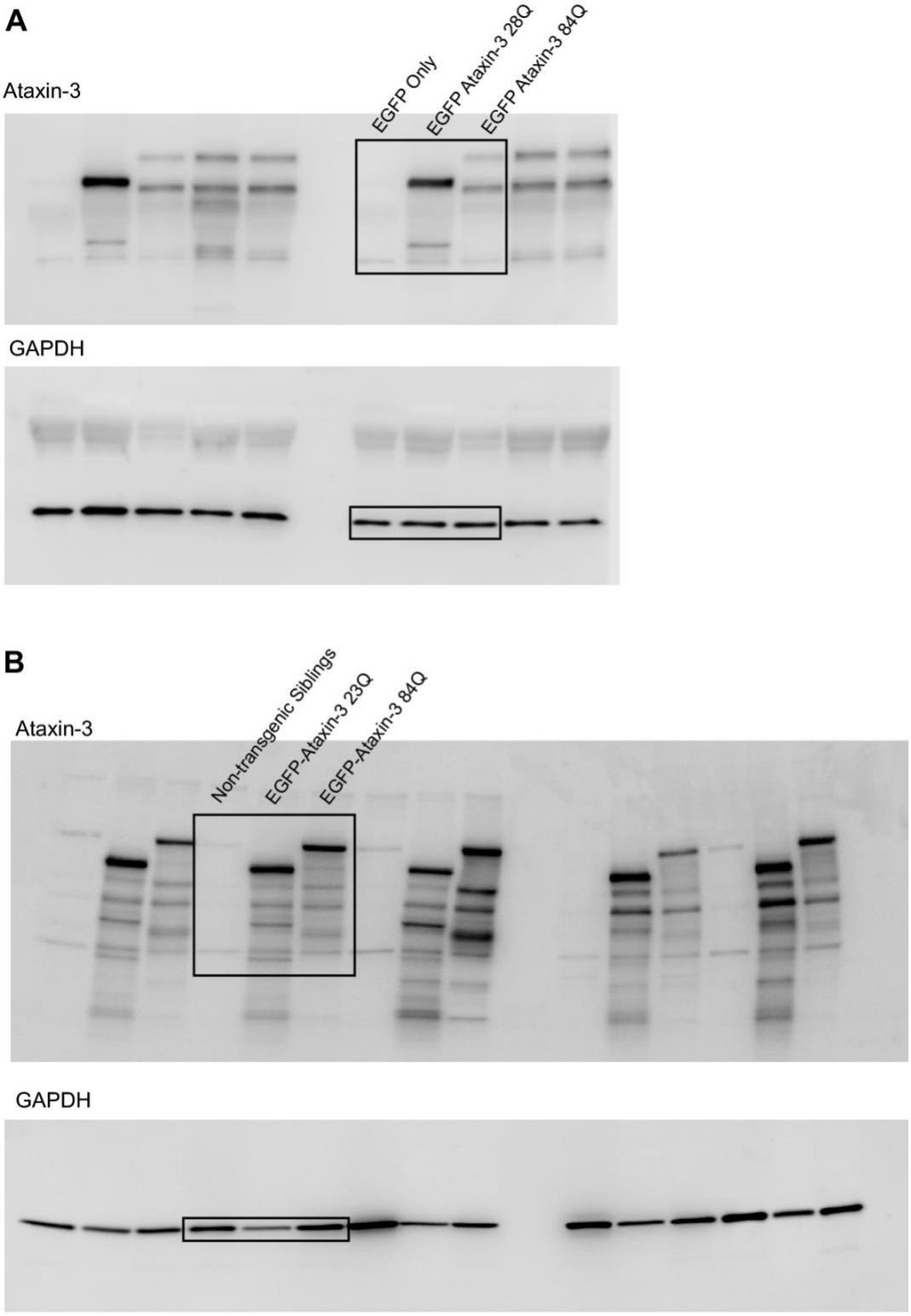

Fig. S2. (A) Uncropped immunoblot images from Figure 1. (B) Uncropped immunoblot images from Figure 4.